Multifragmentation at the balance energy of mass-asymmetric colliding nuclei

Supriya Goyal*
Department of Maths., Stat. and Physics, Punjab Agricultural University, Ludhiana 141 004, India
(Received 19 June 2011; published 21 October 2011)

Using the quantum molecular dynamics model, we study the role of mass asymmetry of colliding nuclei on the fragmentation at the corresponding balance energies and on their mass dependence. The study is done by keeping the total mass of the system fixed as 40, 80, 160, and 240 and by varying the mass asymmetry (defined as $\eta = \frac{A_T - A_P}{A_T + A_P}$; where A_T and A_P are the masses of the target and projectile, respectively) of the reaction from 0.1 to 0.7. Our results clearly indicate a sizeable effect of mass asymmetry on the multiplicity of various fragments. The mass asymmetry dependence of various fragments is found to increase with increase in total system mass (except for heavy mass fragments). Similarly to symmetric reactions, a systematic power-law mass dependence of various fragment multiplicities is also found to exist for large asymmetries.

DOI: 10.1103/PhysRevC.84.044614 PACS number(s): 24.10.Cn, 24.10.Lx, 25.70.Mn, 25.70.Pq

I. INTRODUCTION

The main goals in the study of heavy-ion collisions at intermediate energies are the determination of the bulk properties of nuclear matter or the nuclear equation of state and the understanding of the collision processes which vary over the large range of energies available today. These goals are related to each other and improved insight into one can lead to a better understanding of the other. The study of multifragmentation in the intermediate energy range gives us a possibility to understand the properties of nuclear matter at extreme conditions of temperature and density. The detailed experimental and theoretical studies clearly point toward the dependence of the reaction dynamics on entrance channel parameters such as incident energy and impact parameter, as well as mass asymmetry of the colliding nuclei [1–7].

It is well known that the reaction dynamics for symmetric and asymmetric reactions differ markedly. The former leads to higher compression, whereas the latter has a large share as thermal energy [8]. Asymmetric collisions at relativistic energies were also studied by ISiS and FASA collaborations [9]. Since the model used in the present study does not incorporate relativistic effects, therefore, the present study is limited only for nonrelativistic collisions. In a recent study by Puri and collaboration, a detailed analysis is presented on the effect of mass asymmetry of colliding nuclei on the collective flow and its disappearance, nuclear stopping, elliptical flow, multifragmentation (at fixed energies), and nuclear dynamics [at the balance energy ($E_{\rm bal}$); i.e., energy at which collective flow disappears] by keeping the total mass of the system fixed and at different impact parameters [10,11]. A sizable role of mass asymmetry has been found in all cases. Unfortunately, the role of mass asymmetry of the colliding nuclei on the fragment structure at the balance energy is not presented in the literature.

A similar attempt was made by Dhawan and Puri [12], but it was limited for symmetric colliding nuclei only. Therefore, in the present work, we aim to see the effect of mass asymmetry of the colliding nuclei on the fragment structure and on its mass dependence by simulating the reactions at their corresponding balance energies. The mass asymmetry of the reaction is varied by keeping the total mass of the system fixed. Due to the unavailability of experimental data for the multifragmentation of mass asymmetric collisions at their corresponding balance energies, no comparison is done with the experimental data. The quantum molecular dynamics (QMD) model [1–3,5,6,8,10–14] is used for the present study which has been reported to reproduce the experimental results of the mass and impact parameter dependence of the balance energy (for symmetric systems) [13] and experimental data at low energies [15] very nicely. The present energy domain is <200 MeV/nucleon, therefore, the QMD model is justified. The model is explained in Sec. II. Section III is devoted to the results and discussion followed by summary in Sec. IV.

II. THE MODEL

In quantum molecular dynamics model [1–3,5,6,8,10–14], nucleons (represented by Gaussian wave packets) interact via mutual two- and three-body interactions. Here each nucleon is represented by a coherent state of the form:

$$\phi_i(\vec{r}, \vec{p}, t) = \frac{1}{(2\pi L)^{3/4}} e^{[-\{\vec{r}-\vec{r}_i(t)\}^2/4L]} e^{[i\,\vec{p}_i(t)\cdot\vec{r}/\hbar]}. \quad (1)$$

The Wigner distribution of a system with $A_T + A_P$ nucleons is given by

$$f(\vec{r}, \vec{p}, t) = \sum_{i=1}^{A_T+A_P} \frac{1}{(\pi\hbar)^3} e^{[-\{\vec{r}-\vec{r}_i(t)\}^2/2L]} e^{[-\{\vec{p}-\vec{p}_i(t)\}^2 2L/\hbar^2]'}, \quad (2)$$

with $L = 1.08$ fm^2.

The center of each Gaussian (in the coordinate and momentum space) is chosen by the Monte Carlo procedure. The momentum of nucleons (in each nucleus) is chosen between zero and local Fermi momentum [$=\sqrt{2m_i V_i(\vec{r})}$; $V_i(\vec{r})$ is the potential energy of nucleon i]. Naturally, one has to take care

*supriyagoyal.pu@gmail.com

that the nuclei, thus generated, have right binding energy and proper rms radii.

The centroid of each wave packet is propagated using the classical equations of motion as follows:

$$\frac{d\vec{r}_i}{dt} = \frac{dH}{d\vec{p}_i}, \tag{3}$$

$$\frac{d\vec{p}_i}{dt} = -\frac{dH}{d\vec{r}_i}, \tag{4}$$

where the Hamiltonian is given by

$$H = \sum_i \frac{\vec{p}_i^2}{2m_i} + V^{\rm tot}. \tag{5}$$

Our total interaction potential $V^{\rm tot}$ reads as

$$V^{\rm tot} = V^{\rm Loc} + V^{\rm Yuk} + V^{\rm Coul} + V^{\rm MDI}, \tag{6}$$

with

$$V^{\rm Loc} = t_1\delta(\vec{r}_i - \vec{r}_j) + t_2\delta(\vec{r}_i - \vec{r}_j)\delta(\vec{r}_i - \vec{r}_k), \tag{7}$$

$$V^{\rm Yuk} = t_3 e^{-|\vec{r}_i - \vec{r}_j|/m}/(|\vec{r}_i - \vec{r}_j|/m), \tag{8}$$

with $m = 1.5$ fm and $t_3 = -6.66$ MeV.

The static (local) Skyrme interaction [16] can further be parametrized as

$$U^{\rm Loc} = \alpha\left(\frac{\rho}{\rho_o}\right) + \beta\left(\frac{\rho}{\rho_o}\right)^{\gamma}, \tag{9}$$

where α, β, and γ are the parameters that define equation of state. The momentum dependent interaction is obtained by parameterizing the momentum dependence of the real part of the optical potential. The final form of the potential reads as

$$U^{\rm MDI} \approx t_4 ln^2[t_5(\vec{p}_i - \vec{p}_j)^2 + 1]\delta(\vec{r}_i - \vec{r}_j), \tag{10}$$

where $t_4 = 1.57$ MeV and $t_5 = 5 \times 10^{-4}$ MeV^{-2}. A parameterized form of the local plus momentum-dependent interaction (MDI) potential (at zero temperature) is given by

$$U = \alpha\left(\frac{\rho}{\rho_0}\right) + \beta\left(\frac{\rho}{\rho_0}\right) + \delta ln^2[\epsilon(\rho/\rho_0)^{2/3} + 1]\rho/\rho_0. \tag{11}$$

The parameters α, β, and γ in above Eq. (11) must be readjusted in the presence of momentum-dependent interactions to reproduce the ground-state properties of the nuclear matter. The set of parameters corresponding to different equations of state can be found in Ref. [1].

III. RESULTS AND DISCUSSION

For the present work, we simulated the central reactions of $^{17}_{8}$O + $^{23}_{11}$Na ($\eta = 0.1$, $E_{\rm bal} = 155.8$ MeV/nucleon), $^{14}_{7}$N + $^{26}_{12}$Mg ($\eta = 0.3$, $E_{\rm bal} = 157.4$ MeV/nucleon), $^{10}_{5}$B + $^{30}_{14}$Si ($\eta = 0.5$, $E_{\rm bal} = 163.4$ MeV/nucleon), and $^{6}_{3}$Li + $^{34}_{16}$S ($\eta = 0.7$, $E_{\rm bal} = 184.6$ MeV/nucleon) for $A_{\rm TOT} = 40$, $^{36}_{18}$Ar + $^{44}_{20}$Ca ($\eta = 0.1$, $E_{\rm bal} = 127.3$ MeV/nucleon), $^{28}_{14}$Si + $^{52}_{24}$Cr ($\eta = 0.3$, $E_{\rm bal} = 128.7$ MeV/nucleon), $^{20}_{10}$Ne + $^{60}_{28}$Ni ($\eta = 0.5$, $E_{\rm bal} = 133.1$ MeV/nucleon), and $^{10}_{5}$B + $^{70}_{32}$Ge ($\eta = 0.7$, $E_{\rm bal} = 146.5$ MeV/nucleon) for $A_{\rm TOT} = 80$, $^{70}_{32}$Ge + $^{90}_{40}$Zr ($\eta = 0.1$, $E_{\rm bal} = 102.6$ MeV/nucleon), $^{54}_{26}$Fe + $^{106}_{48}$Cd ($\eta = 0.3$, $E_{\rm bal} = 104.1$ MeV/nucleon), $^{40}_{20}$Ca + $^{120}_{52}$Te ($\eta = 0.5$, $E_{\rm bal} = 108.3$ MeV/nucleon), and $^{24}_{12}$Mg + $^{136}_{58}$Ce ($\eta = 0.7$, $E_{\rm bal} = 121.6$ MeV/nucleon) for $A_{\rm TOT} = 160$, and $^{108}_{48}$Cd + $^{132}_{56}$Ba ($\eta = 0.1$, $E_{\rm bal} = 90.1$ MeV/nucleon), $^{84}_{38}$Sr + $^{156}_{66}$Dy ($\eta = 0.3$, $E_{\rm bal} = 92.7$ MeV/nucleon), $^{60}_{28}$Ni + $^{180}_{74}$W ($\eta = 0.5$, $E_{\rm bal} = 97.3$ MeV/nucleon), and $^{36}_{18}$Ar + $^{204}_{82}$Pb ($\eta = 0.7$, $E_{\rm bal} = 112.7$ MeV/nucleon) for $A_{\rm TOT} = 240$, at their corresponding theoretical balance energies (taken from Ref. [10]). The balance energies at which these reactions are simulated were calculated using a momentum-dependent soft equation of state with a standard energy-dependent Cugnon cross section. The reactions are followed uniformly up to 500 fm/c. A simple spatial clusterization algorithm dubbed as minimum spanning tree (MST) method is used to clusterize the phase space [1].

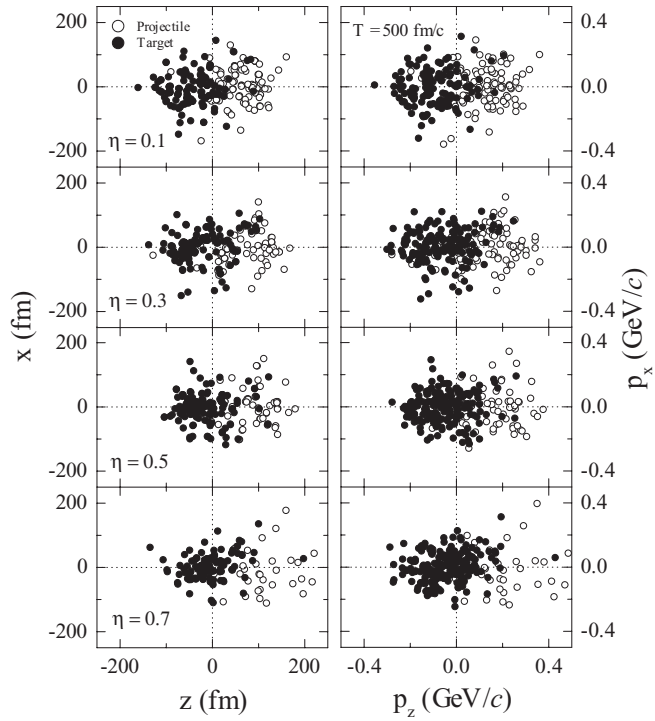

FIG. 1. Snapshots of a single event in the phase space (x, z) (left column) and (p_x, p_z) (right column) for fixed system mass $A_{\rm TOT} = 240$ and $\eta = 0.1$, 0.3, 0.5, and 0.7 at their corresponding balance energies.

In Fig. 1, we display the snapshots of the final phase space [i.e., x, z (left column) and p_x, p_z (right column)] of a single event at the balance energy for $\eta = 0.1$–0.7 by keeping the total mass of the system fixed as $A_{\rm TOT} = 240$. We see an isotropic emission of nucleons for nearly symmetric colliding nuclei, whereas a binary character starts emerging as η increases. One can say that phase space is less homogenous for large asymmetries. The behavior is similar in spatial and momentum spaces. The above picture is quite similar for large number of different events indicating a uniform distribution.

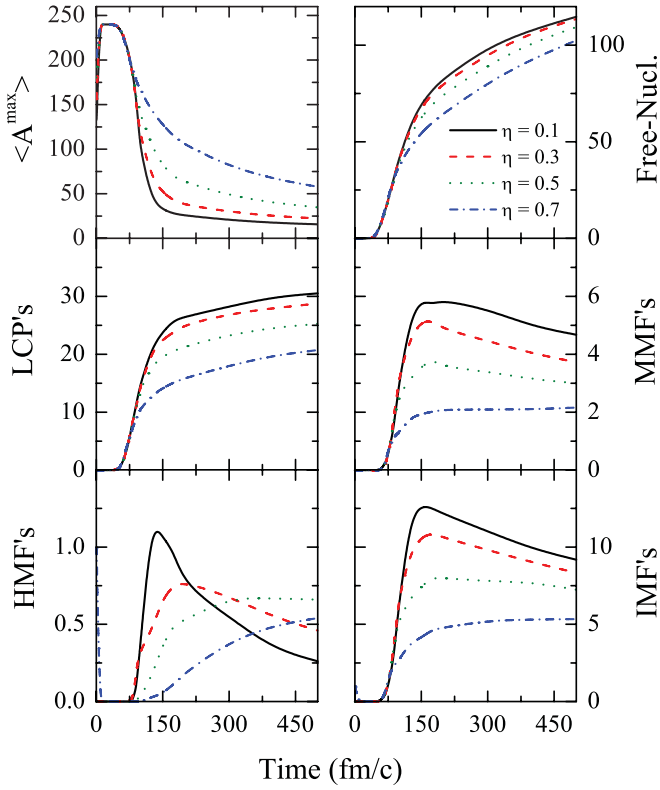

FIG. 2. (Color online) Time evolution of the largest fragment $A^{\max}$, free nucleons, LCP's ($2 \leqslant A \leqslant 4$), MMF's ($5 \leqslant A \leqslant 9$), HMF's ($15\% \leqslant A \leqslant 30\%$), and IMF's ($4 \leqslant A \leqslant 30\%$) for fixed system mass $A_{\mathrm{TOT}} = 240$ and $\eta = 0.1$, 0.3, 0.5, and 0.7 at their corresponding balance energies. The solid, dashed, dotted, and dashed-dotted lines correspond to $\eta = 0.1$, 0.3, 0.5, and 0.7, respectively.

In Fig. 2, we display the time evolution of the largest surviving fragment $\langle A^{\max} \rangle$, free nucleons, the light charged particles (LCP's) $2 \leqslant A \leqslant 4$, the medium mass fragments (MMF's) $5 \leqslant A \leqslant 9$, the heavy mass fragments (HMF's) $15\% \leqslant A \leqslant 30\%$ as well as the intermediate mass fragments (IMF's) $4 \leqslant A \leqslant 30\%$ (of the largest nucleus between target and projectile). The results are displayed for different mass asymmetries by keeping the total mass fixed as $A_{\mathrm{TOT}} = 240$. In order to avoid unwanted and artificial heavy fragments for large asymmetries and lighter colliding nuclei, the percentages are taken in HMF and IMF definitions. As expected, $A^{\max}$ has a peak around 20–80 fm/c for all η. The excited composite nucleus formed in the early stage is independent of η and decays by the emission of nucleons and fragments. Therefore, the free nucleons and LCP's display a constant rise in their multiplicity. It has been observed that there are two phases of light particle emission in the collision. The first, characterized by a prompt emission of light particles and clusters, occurs before the nuclear system is equilibrated and, as such, is often referred to as pre-equilibrium, regardless of its exact and detailed nature. The second phase comes about after complete equilibration of the nuclear system and is accompanied with thermal emission of light and complex particles [17]. One should also note that the early emission of free nucleons

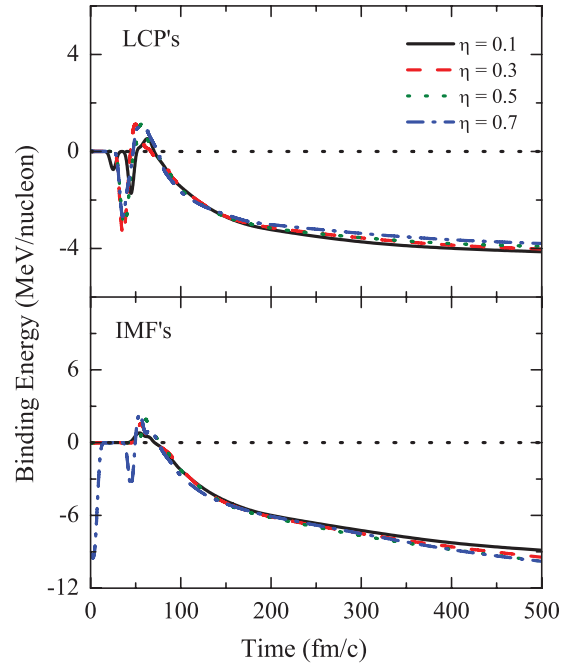

FIG. 3. (Color online) The average binding energy per nucleon of LCP's and IMF's as a function of time for fixed system mass $A_{\mathrm{TOT}} = 240$ and $\eta = 0.1$, 0.3, 0.5, and 0.7 at their corresponding balance energies. Lines have same meaning as in Fig. 2.

and light fragments does not directly influence the emission of fragments during the end of the collision process [7]. In the present study light particle are mainly emitted from the overlap zone, as a consequence of nucleon-nucleon collisions that promptly eject them from the bulk nuclear mean field, which means, a prompt emission of light particles takes place at the highly collisional stage of the reaction. The MMF's, HMF's, and IMF's are unstable and decay at a later time.

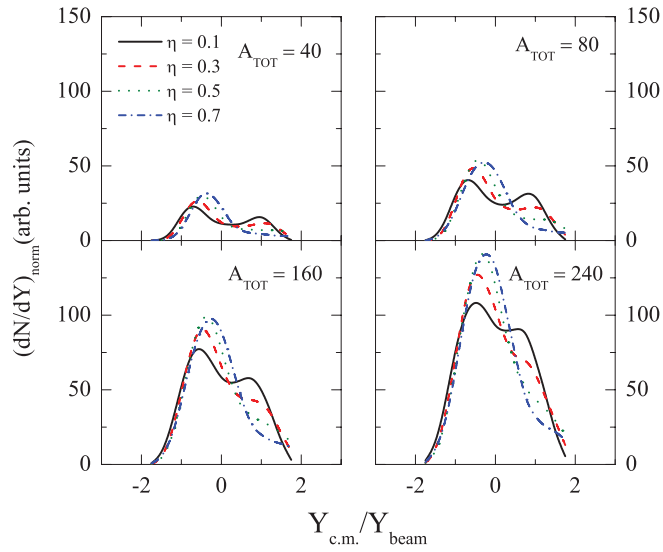

FIG. 4. (Color online) Normalized rapidity distribution $\frac{1}{A_P + A_T} \frac{dN}{dY}$ as a function of scaled rapidity $Y_{\mathrm{c.m.}}/Y_{\mathrm{beam}}$ for $\eta = 0.1$–0.7 by keeping the system mass fixed as $A_{\mathrm{TOT}} = 40$–240. Lines have same meaning as in Fig. 2.

The delayed emission of heavy fragments is mainly coming from the heaviest partner of the reaction. This is similar to as seen for symmetric and asymmetric reactions in Ref. [18]. One should also note that light relativistic projectiles provide a unique possibility for studying thermal multifragmentation, which is not the case in present study. The size of largest fragment at final stage increases with increase in η, whereas a reverse trend is seen for free nucleons, LCP's, MMF's, and IMF's. This is because of the decrease in participant zone and hence net nucleon-nucleon collisions with increase in η. The trend that HMF's follows with η differs. It is clear from the figure that the multiplicity of HMF's increases with time for larger asymmetries. Also, since balance energies for large asymmetric colliding nuclei are larger than for small asymmetric nuclei, it takes lesser time for large asymmetric colliding nuclei to saturate.

In Fig. 3, we display the time evolution of average binding energy per nucleon of LCP's and IMF's for $\eta = 0.1$–0.7 by keeping the total mass fixed as 240. It is clear from the figure that independent of η, all fragments are reasonably bound. The average binding energy per nucleon is around -4 MeV/nucleon for LCP's, whereas it increases to around -8 MeV/nucleon for IMF's.

In Fig. 4, we display the normalized rapidity distribution $[(dN/dY)_{\rm norm}]$ as a function of scaled rapidity $(Y_{\rm c.m.}/Y_{\rm beam})$ for $\eta = 0.1$–0.7 by keeping the system mass fixed as $A_{\rm TOT} =$ 40–240. The rapidity is defined as:

$$Y(j) = \frac{1}{2}\ln\frac{\mathbf{E}(j)+\mathbf{p}_z(j)}{\mathbf{E}(j)-\mathbf{p}_z(j)}. \tag{12}$$

Here $\mathbf{E}(j)$ and $\mathbf{p}_z(j)$ are, respectively, the total energy (nucleon) and longitudinal momentum per nucleon for the jth nucleon. The parameter $Y_{\rm c.m.}/Y_{\rm beam} = 0$ corresponds to the midrapidity (participant) zone and, hence, is responsible for the hot and compressed zone. On the other hand, $Y_{\rm c.m.}/Y_{\rm beam} \neq 0$ corresponds to the spectator zone [$Y_{\rm c.m.}/Y_{\rm beam} < -1$ corresponds to target-like (TL) and $Y_{\rm c.m.}/Y_{\rm beam} > 1$ corresponds to projectile-like (PL) distributions]. We see that the rapidities of nucleons emitted for $\eta = 0.1$–0.7 are not similar. Due to large balance energy for larger asymmetries, single broader Gaussian is observed which is peaked around the target rapidity, as the major contribution is due to the target in all cases. As mass asymmetry decreases, the balance energy decreases, therefore, one find peaks at target and projectile rapidities indicating a nonequilibrium situation. However, if the reactions would have been simulated at a fixed incident energy, the peaks shift toward the midrapidity with the decrease of the mass asymmetry and a greater thermalization would have been observed in the case of a nearly symmetric collision

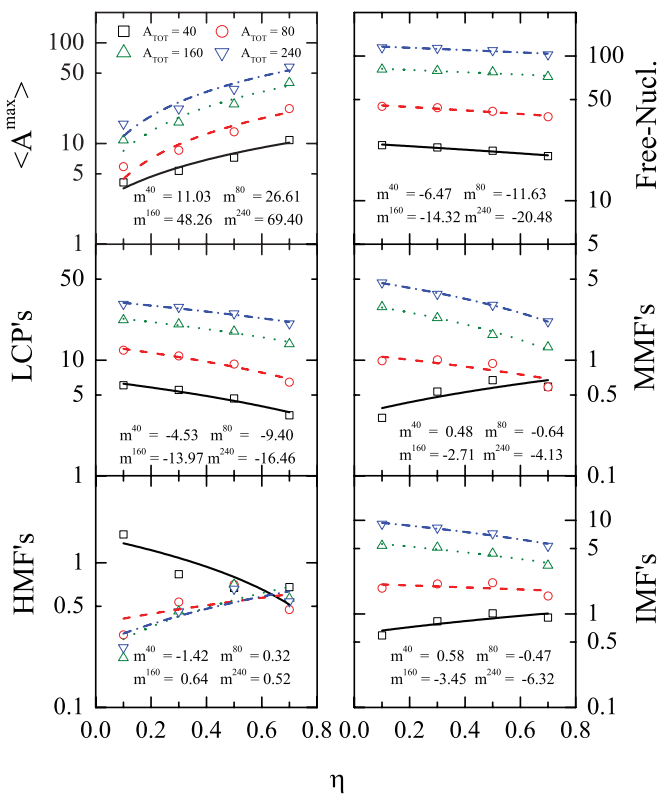

FIG. 5. (Color online) The multiplicities of $A^{\rm max}$, free nucleons, LCP's, MMF's, HMF's, and IMF's as a function of mass asymmetry of colliding nuclei. The results for different system masses $A_{\rm TOT} =$ 40, 80, 160, and 240 are represented, respectively, by the open squares, circles, triangles, and inverted triangles. Lines are the linear fits ($\propto m\eta$); m values without errors are displayed.

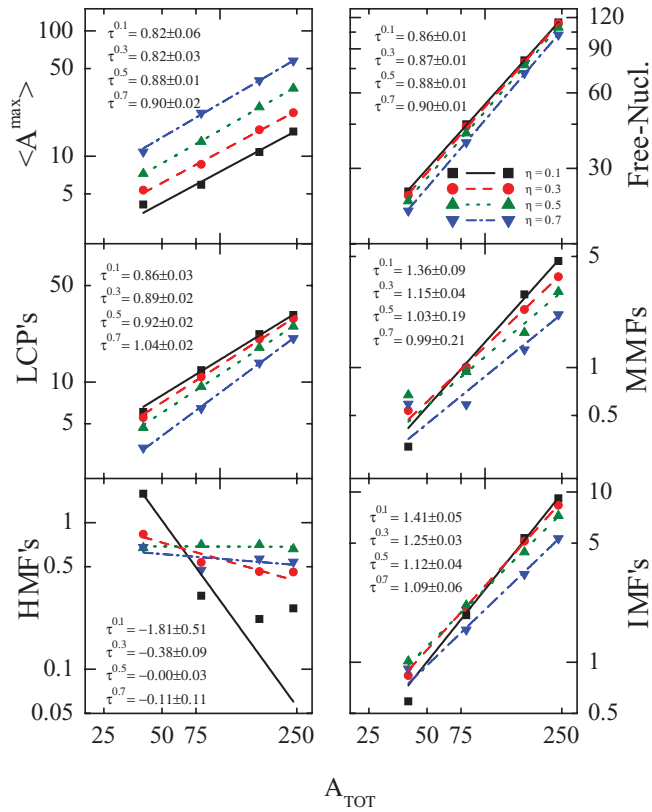

FIG. 6. (Color online) Same as Fig. 5 but as a function of total mass of the system. The results for different asymmetries $\eta = 0.1$, 0.3, 0.5, and 0.7 are represented, respectively, by the solid squares, circles, triangles, and inverted triangles. The lines are power law ($\propto A_{\rm TOT}^{\tau}$) fits to the calculated results. The values of the power factor τ are displayed in the figure for various quantities.

compared to an asymmetric collision. The same trend is seen for all fixed system masses.

In Fig. 5, we display the mass asymmetry dependence of different fragments shown in Fig. 2 for $A_{\rm TOT} = 40$–240. Lines are the linear fits ($\propto m\eta$). The values of m are displayed in figure. The mass of the largest fragment increases with increase in η for each $A_{\rm TOT}$, whereas an opposite trend is seen for free nucleons, LCP's, MMF's (except $A_{\rm TOT} = 40$), and IMF's (except $A_{\rm TOT} = 40$). The multiplicity of HMF's show entirely different behavior. It is clear from the figure that η dependence increases with increase in system mass. This is because of decrease in balance energy with increase in $A_{\rm TOT}$. At low incident energies, the Pauli principal hinders the nucleon-nucleon collisions and the increase of mass asymmetry further adds the same effect. While at large incident energies for smaller $A_{\rm TOT}$, the role of η decreases compared to large system masses.

Similar to Fig. 5, we display the mass dependence of various fragments in Fig. 6. The mass asymmetry of the reaction is varied from 0.1 to 0.7. Lines are power-law fits ($\propto A_{\rm TOT}^{\tau}$); where values of power factor τ are displayed in the figure. Similarly to mass symmetric reactions [12], a power-law system mass dependence for various fragment multiplicities exists for larger asymmetries. All the quantities except HMF's show increasing trends for each η. It is clear from the values of τ that, for $A^{\rm max}$, free nucleons, and LCP's; the mass dependence increases with increase in η, whereas the opposite trend is seen for MMF's, HMF's, and IMF's. The trend of MMF's, HMF's and IMF's with change in η from 0.1 to 0.7 in the lighter mass range gets reversed as one goes to higher mass range. This is because for lighter system mass, the incident energy is large compared to heavier system mass, therefore, large mass asymmetric colliding nuclei will produce more heavy fragments. The situation is entirely opposite for heavier system mass.

IV. SUMMARY

We presented the study of role of mass asymmetry of colliding nuclei on the fragmentation at the balance energy and on its mass dependence using a quantum molecular dynamics model. The analysis was done by keeping the total mass of the system fixed as 40, 80, 160, and 240 and by varying the mass asymmetry of the colliding nuclei from 0.1 to 0.7. We find a sizable effect of the mass asymmetry on the multiplicity of various fragments. Our finding at the balance energy clearly points toward a power-law system mass dependence of different fragment multiplicities for each mass asymmetric colliding nuclei.

AKNOWLEDGMENT

The author is thankful to Dr. Rajeev K. Puri at the Physics Department of Panjab University (Chandigarh) for interesting and constructive discussions.

[1] J. Aichelin and H. Stöcker, Phys. Lett. B **176**, 14 (1986); J. Aichelin, Phys. Rep. **202**, 233 (1991).

[2] H. Feldmeier, Nucl. Phys. A **515**, 147 (1990); B. Jakobsson *et al.*, *ibid.* **509**, 195 (1990); H. W. Barz *et al.*, *ibid.* **548**, 427 (1992); A. Ono, H. Horiuchi, and T. Maruyama, Phys. Rev. C **48**, 2946 (1993); J. Schnack, Ph.D. thesis, Technische Universität Darmstadt, 1996.

[3] Li Zhuxia, C. Hartnack, H. Stöcker, and W. Greiner, Phys. Rev. C **44**, 824 (1991); P. B. Gossiaux, R. K. Puri, C. Hartnack, and J. Aichelin, Nucl. Phys. A **619**, 379 (1997); C. Hartnack *et al.*, Eur. Phys. J. A **1**, 151 (1998); S. Kumar and R. K. Puri, Phys. Rev. C **58**, 2858 (1998); **60**, 054607 (1999).

[4] C. A. Ogilvie *et al.*, Phys. Rev. Lett. **67**, 1214 (1991); R. T. de Souza *et al.*, Phys. Lett. B **268**, 6 (1991); J. Hubble *et al.*, Z. Phys. A **340**, 263 (1991); M. B. Tsang *et al.*, Phys. Rev. Lett. **71**, 1502 (1993); W. J. Llope *et al.*, Phys. Rev. C **51**, 1325 (1995); C. Williams *et al.*, *ibid.* **55**, R2132 (1997); N. T. B. Stone *et al.*, Phys. Rev. Lett. **78**, 2084 (1997).

[5] S. Kumar, M. K. Sharma, R. K. Puri, K. P. Singh, and I. M. Govil, Phys. Rev. C **58**, 3494 (1998); S. Kumar, R. K. Puri, and J. Aichelin, *ibid.* **58**, 1618 (1998); J. K. Dhawan and R. K. Puri, *ibid.* **75**, 057601 (2007); **75**, 057901 (2007); S. Kumar, S. Kumar, and R. K. Puri, *ibid.* **78**, 064602 (2008); **81**, 014601 (2010).

[6] R. K. Puri, C. Hartnack, and J. Aichelin, Phys. Rev. C **54**, R28 (1996); R. K. Puri and S. Kumar, *ibid.* **57**, 2744 (1998); R. K. Puri *et al.*, J. Comput. Phys. **162**, 245 (2000); Y. K. Vermani *et al.*, J. Phys. G **36**, 105103 (2009); Europhys. Lett. **85**, 062001 (2009); Y. K. Vermani, S. Goyal, and R. K. Puri, Phys. Rev. C **79**, 064613 (2009); Y. K. Vermani *et al.*, J. Phys. G **37**, 015105 (2010); S. Kumar, S. Kumar, and R. K. Puri, Phys. Rev. C **81**, 014611 (2010); S. Goyal and R. K. Puri, *ibid.* **83**, 047601 (2011).

[7] K. Turzo, Ph.D. thesis, Université Claude Bernard-Lyon I, 2002.

[8] J. Singh, Ph.D. thesis, Panjab University, Chandigarh, India, 2001.

[9] K. Kwiatkowski *et al.*, Phys. Lett. B **423**, 21 (1998); S. P. Avdeyev *et al.*, Eur. Phys. J. A. **3**, 75 (1998).

[10] S. Goyal and R. K. Puri, Nucl. Phys. A **853**, 164 (2011).

[11] V. Kaur and S. Kumar, Phys. Rev. C **81**, 064610 (2010); S. Goyal, Nucl. Phys. A **856**, 154 (2011); Phys. Rev. C **83**, 047604 (2011); V. Kaur, S. Kumar, and R. K. Puri, Phys. Lett. B **697**, 512 (2011); Nucl. Phys. A **861**, 37 (2011); S. Goyal, *ibid.* (2011), submitted.

[12] J. K. Dhawan and R. K. Puri, Phys. Rev. C **74**, 054610 (2006).

[13] A. D. Sood and R. K. Puri, Phys. Lett. B **594**, 260 (2004); Phys. Rev. C **69**, 054612 (2004); **70**, 034611 (2004); Eur. Phys. J. A **30**, 571 (2006); Phys. Rev. C **73**, 067602 (2006); **79**, 064618 (2009); R. Chugh and R. K. Puri, *ibid.* **82**, 014603 (2010).

[14] S. W. Huang *et al.*, Phys. Lett. B **298**, 41 (1993); Prog. Nucl. Part. Phys. **30**, 105 (1993); E. Lehmann *et al.*, *ibid.* **30**, 219 (1993); G. Batko *et al.*, J. Phys. G **20**, 461 (1994); E. Lehmann, R. K. Puri, A. Faessler, G. Batko, and S. W. Huang, Phys. Rev. C **51**, 2113 (1995); C. Fucks, J. Phys. G **22**, 131 (1996); S. Gautam *et al.*, *ibid.* **37**, 085102 (2010); S. Gautam, A. D. Sood,

R. K. Puri, and J. Aichelin, Phys. Rev. C **83**, 014603 (2011); **83**, 034606 (2011); W. Hauer *et al*., Phys. Lett. B **697**, 512 (2011).

[15] P. B. Gossiaux and J. Aichelin, Phys. Rev. C **56**, 2109 (1997); J. Singh, S. Kumar, and R. K. Puri, *ibid*. **62**, 044617 (2000); J. Singh and R. K. Puri, *ibid*. **62**, 054602 (2000); S. Kumar and R. K. Puri, *ibid*. **58**, 320 (1998).

[16] R. K. Puri, P. Chattopadhyay, and R. K. Gupta, Phys. Rev. C **43**, 315 (1991); R. K. Puri and R. K. Gupta, *ibid*. **45**, 1837 (1992); R. K. Puri *et al*., Eur. Phys. J. A **3**, 277 (1998); **8**, 103 (2000); **23**, 429 (2005); I. Dutt and R. K. Puri, Phys. Rev. C **81**, 044615 (2010); **81**, 047601 (2010); **81**, 064609 (2010); **81**, 064608 (2010); S. Kumar *et al*., Chin. Phys. Lett. **27**, 062504 (2010).

[17] A. Malki *et al*., Z. Phys. A-Hadron Nucl. **339**, 283 (1991).

[18] A. Chernomoretz *et al*., Phys. Rev. C **65**, 054613 (2002); J. K. Dhawan *et al*., *ibid*. **74**, 057901 (2006); V. Kaur and S. Kumar, arXiv:1109.3949v1 [nucl-th].